Journal of Molecular Graphics and Modelling 27 (2008) 536–545

Contents lists available at ScienceDirect

Journal of Molecular Graphics and Modelling

journal homepage: www.elsevier.com/locate/JMGM

Binding of the tautomeric forms of isoniazid-NAD adducts to the active site of the *Mycobacterium tuberculosis* enoyl-ACP reductase (InhA): A theoretical approach

Jean-Luc Stigliani, Philippe Arnaud, Tamara Delaine, Vania Bernardes-Génisson, Bernard Meunier [1], Jean Bernadou *

Laboratoire de Chimie de Coordination du CNRS, 205 route de Narbonne, 31077 Toulouse Cedex 4, France

ARTICLE INFO

Article history:
Received 29 July 2008
Received in revised form 4 September 2008
Accepted 5 September 2008
Available online 17 September 2008

Keywords:
Isoniazid
Tuberculosis
InhA inhibitors
Computer chemistry
Tautomerism

ABSTRACT

The front-line antituberculosis drug isoniazid (INH) inhibits InhA, the NADH-dependent fatty acid biosynthesis enoyl ACP-reductase from *Mycobacterium tuberculosis*, via formation of covalent adducts with NAD (INH-NAD adducts). While ring tautomers were found the main species formed in solution, only the 4*S* chain INH-NAD tautomer was evidenced in the crystallized InhA:INH-NAD complex. In this study we attempted to explore the modes of interaction and energy binding of the different isomers placed in the active site of InhA with the help of various molecular modelling techniques. Ligand and enzyme models were generated with the help of the Vega ZZ program package. Resulting ligands were then docked into the InhA active site individually using computational automated docking package AUTODOCK 3.0.5. The more relevant docked conformations were then used to compute the interaction energy between the ligands and the InhA cavity. The AM1 Hamiltonian and the QM/MM ONIOM methodologies were used and the results compared. The various tautomers were found docked in almost the same place where INH-NAD was present as predicted by earlier X-ray crystallographic studies. However, some changes of ligand conformation and of the interactions ligand–protein were evidenced. The lower binding energy was observed for the 4*S* chain adduct that probably represents the effective active form of the INH-NAD adducts, as compared to the 4*R* epimer. The two 4*S*,7*R* and 4*R*,7*S* ring tautomers show intermediate and similar binding energies contrasting with their different experimental inhibitory potency on InhA. As a possible explanation based on calculated conformations, we formulated the hypothesis of an initial binding of the two ring tautomers to InhA followed by opening of only the ring hemiamidal 4*S*,7*R* tautomer (possibly catalyzed by Tyr158 phenolate basic group) to give the 4*S* chain INH-NAD tight-binding inhibitor. The predictions of ligand–protein interactions at the molecular level can be of primary importance in elucidating the mechanisms of action of isoniazid and InhA-related resistances, in identifying the effective mycobactericidal entities and, in further step, in the design of a new generation of antitubercular drugs.

1. Introduction

Isoniazid (INH) (Fig. 1) is one of the most common and efficient drugs used in treatment of tuberculosis [1,2]. After activation by the catalase-peroxydase KatG [3–7], it inhibits enoyl-acyl carrier protein reductase InhA, an enzyme involved in the fatty acid biosynthesis (FAS II system), which is an essential process to elaborate important cellular components of *Mycobacterium tuberculosis* [8,9].

Data from X-ray crystallography [10], mass spectrometry [11] and isotopic experiments [12] reveal that the mechanism of the inhibition involves a covalent attachment of the activated form of the drug (isonicotinoyl radical) to the nicotinamide ring of nicotinamide adenine dinucleotide NAD(H) modifying thereby the nature of the coenzyme and its interaction with the target enzyme InhA. Recent studies have suggested that the 1,4-dihydropyridine INH-NAD adduct exhibits the keto-carboxamide structure **3** (Fig. 2) [10,13,14]. On the other hand, our group has reported that the biomimetic activation of INH with manganese(III) pyrophosphate in the presence of the coenzyme NAD^+ **1** (Fig. 1) results mainly in formation of the ring hemiamidal dihydropyridines **6** and **7** (with creation of two new chiral centers

* Corresponding author. Fax: +33 5 61 55 30 03.
E-mail address: bernadou@lcc-toulouse.fr (J. Bernadou).
[1] New address: Palumed, BP 28262, 31682 Labège Cedex, France.

1093-3263/$ – see front matter © 2008 Elsevier Inc. All rights reserved.
doi:10.1016/j.jmgm.2008.09.006

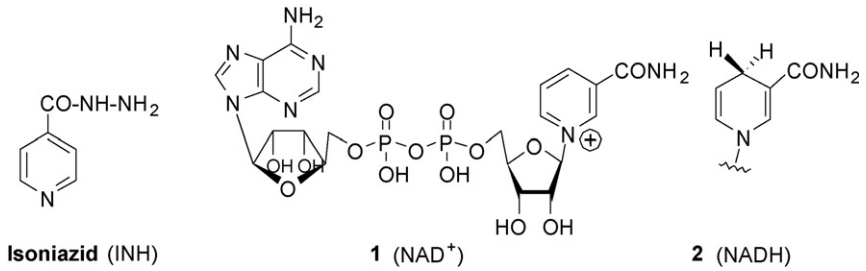

Fig. 1. Structures of isoniazid and of the two redox cofactors NAD^+ and NADH.

at C-4 and C-7 to give four diastereoisomers) along with the chain keto-amide structures **3** and **4** as minor compounds (two epimers 4*S* and 4*R*) [15,16]. It is interesting to note that a purified pool of all these adducts have been shown to be effective inhibitors of InhA [17]. The key structural factors involved in the ring–chain tautomerism equilibrium has been discussed on a series of simplified analogues of isoniazid-NAD adducts [18]. Rawat et al. [19] have reported that the analogue of INH-NAD adduct derived from metabolic activation of benzoylhydrazine (BH-NAD **5**; Fig. 2), with a proposed chain (keto-amide) structure, behaves also as a potent inhibitor of InhA. On the other hand, slow oxidation of the dihydropyridine INH-NAD adducts can afford oxidized derivatives of a pyridinium type which structure was initially proposed to be **10** [13]. However, our recent results show unambiguously their existence under only the two epimeric ring structures **8** and **9** [16].

Recently, it was suggested that the difference between bactericidal (FAS I and FAS II systems) and mammalian (FAS I system) fatty acid biosynthesis makes InhA an attractive molecular target whose selective inhibition is sought in the development of antibiotics with new mechanism of action. In addition, it was observed that the high prevalence of resistances to INH was mainly due to KatG mutants that could not activate isoniazid. Hence, direct inhibitors of InhA not KatG-dependent have been considered as promising antitubercular agents.

Computer-aided drug design approaches are a powerful tool for a better knowledge of the biological effects of molecules. In a recent study [20], Pasqualoto et al. performed a 4D-QSAR analysis of a set of INH analogues hydrazides, which led the authors to develop a 3D pharmacophore model. The resulting hypothesized active conformations were then used as point of departure in molecular dynamics simulations to generate a 3D-QSAR model [21], which allowed them to identify the critical thermodynamic descriptors. In another recent article [22], Bonnac et al. carried out comparative docking experiments of chain INH-NAD adducts and the 4-phenoxybenzamide adenine dinucleotide analogue in interaction with InhA. As part of our effort to develop direct inhibitors of InhA based on the understanding of isoniazid mechanism [23–25] and since computer-aided drug design approaches are widely used to simulate molecular interactions of large systems, we envision in this work to compute the molecular interactions associated with the binding of the chain and ring INH-NAD tautomers to InhA. These studies can be of primary importance in to elucidate the mechanism of action of isoniazid and to better understand the isoniazid-dependent resistances. They can also prove useful in the design of a new generation of antitubercular drugs.

2. Materials and methods

All calculations were performed on a SGI Altix 3700 cluster at Toulouse University Computer Center (France) and locally on PC workstations.

2.1. Protein and ligands structures

The coordinates of INH-NAD adduct complexed to InhA were taken from the Brookhaven Protein Data Bank (PDB code 1ZID) [10]. The adduct was extracted from the PDB file and hydrogen atoms were added to the protein and oriented using the MolProbity software [26]. Hydrogens were added on the crystal structure of INH-NAD adduct and energy-minimized using the AMMP [27] force field implemented on the VEGA ZZ [28] molecular modelling package. The coordinates of the other studied adducts were built from the NADH moiety of the INH-NAD which was kept unchanged. Only the variable part of the molecules was energy-minimized.

2.2. Autodock docking study

The docking studies were performed with the program Autodock version 3.0.5 [29]. Water molecules were discarded, except those surrounding the binding site (i.e. water molecules

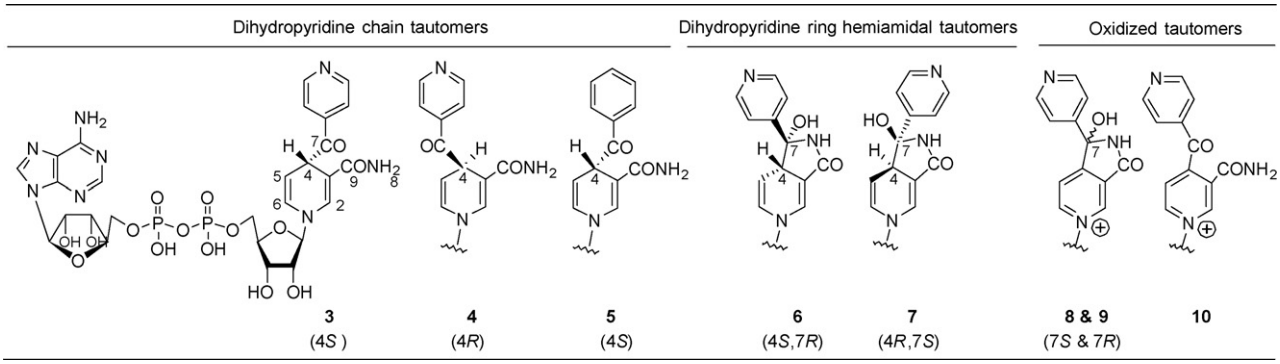

Fig. 2. Structures of compounds **3**–**10** with mention of the proposed stereochemistry of new chiral centers. Dihydropyridine ring hemiamidal tautomers 4*S*,7*S* and 4*R*,7*R* were only detected as traces and are not studied here.

403, 404, 424, 429, 436, 437, 453 and 455) which were observed in various NAD-bound enoyl ACP reductases crystal structures: 1ENY [30], 1ENZ [30], 1BVR [31] (*M. tuberculosis*); 1LXC [32] (*Escherichia coli* FabI); 1NHG [33] (*Plasmodium falciparum*). One can notice that, for all these enzymes, the NAD cofactor positions in a superimposable manner in the binding site; this is also true for the INH-NAD adduct whose NAD moiety fits the site of the cofactor. The Autodock graphical interface AutoDockTools [34,35] was used to keep polar hydrogens and add partial charges for protein using the Kollman United charges. Atomic solvation parameters and fragmental volumes were assigned using the ADDSOL subroutine. The grid maps were calculated using the auxiliary program Autogrid 3.0.6. Grid maps of $70 \times 70 \times 70$ points centered on the binding site of the ligand with 0.375 Å spacing were calculated for each of the atom types found on the adducts. Lamarckian genetic algorithm (LGA) was selected for ligand conformational searching. Default parameters were used, except for the number of energy evaluations and docking runs, which were set to 2,000,000 and 200, respectively. The resulting docked conformations were clustered into families of similar conformations, with a root mean square deviation (RMSD) clustering tolerance of 0.5 Å. As a rule, the lowest docking-energy conformations were included in the largest cluster. Flexible torsions in the ligands were assigned with Autotors, an auxiliary module of AutoDockTools. Insofar as we consider that the NAD moiety of the whole studied adducts fits in the same manner as the cofactor, the only dihedral angles allowed to rotate freely were those belonging to the acylated nicotinamide moiety of the adducts, excluding amide bonds. In this manner we reduced the number of torsions, which is of 18 on the entire adduct. Partial charges fitted to the electrostatic potential were computed with the Merz–Singh–Kollman method [36] at the HF/6-31G(d) level with Gaussian 03 [37]. In all the calculations, the global charge of the adducts was set to – 2 for dihydropyridine derivatives and to – 1 for the pyridinium ones, considering that the two phosphate groups of the NAD part were deprotonated.

2.3. AM1 model and conception of the rigid model receptor

From the protonated protein, amino acid residues and water molecules centered on the binding site of the ligand and included in a sphere of about 25 Å were selected. All the other residues were discarded. The valences of broken –CO–NH– amide bonds were completed as $-CO-NH_2$ or –NH–CHO. The system so defined contains 61 residues or 860 atoms. For each studied ligand, the more relevant docked conformations were merged in the cavity using the VEGA ZZ software. The structure of the receptor was kept fixed while the ligand was energy-minimized with the AMMP force field. The derived ligand–receptor complexes were next submitted to a gradient energy calculation with the semi-empirical AM1 and PM3 [38,39] Hamiltonians implemented in the PC GAMESS [40] version 7.0 of the GAMESS (US) quantum chemistry package [41]. The Pulay's convergence acceleration algorithm [42] was used (DIIS = true). The energy interaction was then calculated with the equation: $\Delta E = \Delta H_f$ (ligand–receptor complex) $- \Delta H_f$ (ligand) $- \Delta H_f$ (receptor). For each ligand, the better result was then kept (Table 1). One can notice that the AMMP minimization step of the ligand into the cavity was justified by the better results obtained with AM1/PM3 in comparison with the energy calculation directly performed on the corresponding adducts issued from AutoDock calculations.

2.4. Two-layer ONIOM methodology

The hybrid quantum mechanical and molecular mechanical methodologies (QM/MM) use different levels of method for different parts of a molecule. They treat a localized region, e.g. the active site of the enzyme, with QM methods and include the influence of the surroundings, e.g. the protein environment at the MM level. In this work we used the two-layer ONIOM method [43,44]. In the ONIOM terminology, the *real system* refers to the entire system and is treated at a low-level MM method. The *model system* which in our case summarizes the adduct is treated both at a high-level QM and low-level MM. The energy of the entire system at the high level can be estimated by: E(ONIOM,real) = E(high,-model) + E(low,real) – E(low,model). The model system (i.e. the adduct) was fully optimized at the B3LYP/6-31G(d) [45] level while the real system was treated with the Amber [46] force field, using the Gaussian 03 program package. The QM/MM interaction was treated by mechanical embedding. For this study, we used the entire InhA 1ZID with all the water molecules. Hydrogen atoms were added using GaussView program [47]. The adducts included in the ONIOM model were those which gave the best result in the rigid model study. The atomic parameters required to describe these adducts have been obtained from the general Amber force field (GAFF) [48]. The atomic partial charges were computed at the B3LYP/6-31G(d) level with Gaussian 03 [37].

2.5. Molecular dynamics (MD) simulations

The crystal structure geometries of the wild-type InhA:INH-NAD complex **3** [10] were taken as the starting points for MD simulations of the complexes. Exploiting the possibility of combining two parameters set in one simulation, we used the parm99 force field for the protein and GAFF parameters for the ligand. Atomic charges of adducts were assigned by ab initio calculations at the HF/6-31G(d) level. RESP charges [49] were subsequently calculated using Antechamber in Amber 7. To neutralize the charge of the system, an appropriate number of sodium counter-ions were added. The complexes were subsequently surrounded with a box of TIP3P water molecules extending to 10 Å from the complex. The number of water molecules in the box was 10,544 and the approximate size of the boxes was 78 Å × 73 Å × 77 Å. Water molecules obtained by crystallographic structure were kept. The simulation protocol involved a series of progressive energy minimizations followed by a 20-ps heating phase and a 50-ps equilibration period before data collection. During the minimization step, the water box was subjected to five rounds of minimization during which harmonic restraints on the solutes and counterions were reduced from 100 kcal/(mol·Å^2) to 0. The steps of minimization were followed by 70 ps of MD, during which the temperature was slowly raised from 0 to 300 K over 20 ps. Positional constraints were applied to the atoms during thermalization and gradually reduced during the last 50 ps of equilibration. The unrestrained molecular dynamics were performed at 300 K and a constant pressure of 1.0 atm with isotropic position scaling using Berendsen algorithm for temperature coupling [50].

Molecular dynamics (MD) simulations were carried out by using the Sander module of Amber 7.0 with SHAKE [51] applied to all hydrogen atoms and 2 fs time steps. Long-range electrostatic forces were evaluated using the particle mesh Ewald method [52,53]. A 9-Å cutoff was applied to the Lennard–Jones interactions. System coordinates were saved every 0.2 ps. RMSD from the initial structures, interatomic distances and average structures from the trajectories were calculated using the Carnal and Ptraj modules of Amber.

The binding free energy was computed by the difference between the protein, the adduct and their complex of a single MD simulation, where the protein and adduct were taken from the complex simulation. The various MM-GBSA energy terms were

Table 1
Docking/interaction energies of compounds 1–9 bound to InhA calculated with various methods.

	Stereochemistry on nicotinamide moiety	Autodock binding energy (kcal/mol)	Autodock number of clusters[a]	Autodock number of results[b]	Relative interaction energy (kcal/mol)				% Inhibition of InhA	InhA affinity (K_D or K_i)[c]
					Autodock	AM1	ONIOM	MM/GBSA		
1	–	−17.7	8	174	6.3	29	136	NC	–	K_i 4 mM [56]
2	–	−18.5	5	140	5.5	9.4	50	NC	–	K_D 2 μM [30,56]
3^{cryst}	4*S*	−22.8	–	–	1.2	30.1	NC	NC	–	
3^{calc}	4*S*	−24	4	182	0	0	0	0	ND	On a mixture
4	4*R*	−22	5	184	2	11.1	23	2.5	ND	of isomers: $K_D < 0.4$ nM
5	4*S*	−23.3[d]	4	158	0.7[d]	0[d]	5[d]	NC	ND	[11] K_i 100 nM [13]
6	4*S*,7*R*	−21.3	7	49	2.7	5.1[e]	47	4.2	71 [17]	K_i 16 nM/0.75 nM [19]
7	4*R*,7*S*	−23.2	5	110	0.8	6.2[f]	55	1.5	31 [17]	
8	7*S*	−20.4	4	128	3.6	34.7	NC	NC	On **8** + **9**: 0 [13,16]	
9	7*R*	−20.7	3	143	3.3	49.9	NC	NC		

NC: not calculated; ND: not determined.
[a] With a RMSD tolerance of 0.5 Å and 200 trials.
[b] in the top-ranked cluster.
[c] From literature data.
[d] Calculated without water 403.
[e] 8.0 when 7-OH was removed and replaced by 7-H.
[f] 5.2 when 7-OH was removed and replaced by 7-H.

calculated as follows: $\Delta G_{binding} = \Delta E_{gas} + \Delta G_{sol} - T\Delta S$ where molecular mechanics interaction energy in the gas phase (ΔE_{gas}) can be decomposed into electrostatic energy and van der Waals energies, $\Delta E_{gas} = \Delta E_{ele} + E_{vdw}$ and was evaluated using the SANDER module. The solvation free energy (ΔG_{sol}) was estimated by continuum solvent methods as the sum of electrostatic (ΔG_{polar}) and nonpolar ($\Delta G_{nonpolar}$) contributions. The electrostatic contribution to the solvation free energy (ΔG_{polar}) was calculated by GB model as implemented in SANDER, applying dielectric constants of 1 and 80 to represent the solute and the exterior medium phases, respectively. Nonpolar components ($\Delta G_{nonpolar}$), is represented as $G_{nonpolar} = \gamma SASA + b$, where $\gamma = 0.0072$ kcal/Å^2 and $b = 0.0$ kcal/mol. Solvent accessible surface area (SASA) was estimated with the program MSMS [54]. Because this first theoretical study was more qualitative than quantitative analysis and also in reason of time-consuming of entropy contribution to the binding free energy, $T\Delta S$ was not considered in our calculations. Free binding energy given as relative to the lowest energy value were calculated and analysed. Three-dimensional structures and trajectories were displayed using the computer graphics program VMD [55].

3. Results and discussion

The computer simulated automated docking studies were initially performed using the molecular docking software AutoDock 3.0.5 [29]. Although AutoDock is the most widely used docking program and it has been extensively validated, the reliability of purpose, the crystalline structure of INH-NAD inhibitor **3**^{cryst} (Fig. 3) obtained by X-Ray diffraction of the enzyme InhA with INH-NAD inhibitor bound in the active site was used as starting point for the docking studies (PDB 1ZID) [10]. In the case of adduct **3**, designation **3**^{cryst} and **3**^{calc} are used to distinguish the crystalline and calculated conformations. In a first time, the Autodock single point calculation was applied to the native crystal structure **3**^{cryst} after addition and relaxation of polar hydrogen atoms without any other modification. The calculated docking energy was −22.8 kcal/mol (Table 1). Taking into account that rotations can occur around the bond between the isonicotinoyl group and C-4 atom of the nicotinamide ring and around the C–CO bond of the isonicotinoyl, the docking energy for the inhibitor adduct was then recalculated allowing free rotation around these bonds.

Since the NAD group was found in similar conformations in several enoyl-ACP reductases crystal structures, this molecular component was kept rigid (see Section 2). Therefore, the ligand is partially flexible (isonicotinoyl-nicotinamide moiety) and the protein is held rigid. In these last conditions, the INH-NAD adduct **3** showed a lowered $E_{docking}$ of −24.0 kcal/mol. With respect to the modified part of NAD in the adduct (acylated nicotinamide), the main difference with **3**^{cryst} was a reversal of the orientation of the amide moiety (Fig. 3). Critical interactions with protein were:

- H-bonds between Ile194 and the amido NH_2 group of nicotinamide (C═O$_{ile}$...NH–H, N–H$_{ile}$...NH_2–CO);
- interaction of the isonicotinoyl nitrogen with Met155 through H-bonding with water 403;
- π–π stacking of the pyridine ring of the isonicotinoyl part with the phenyl ring of Phe149.

However, while in both adducts **3**^{cryst} and **3**^{calc} the distance between the aromatic rings was quite identical, a main difference appeared for **3**^{calc} with a torsion of the isonicotinoyl ring of 38° (dihedral angle) that reduces the π–π stacking with Phe149 (Table 2).

In these conditions, the conformation **3**^{calc} was found to bind more favourably than **3**^{cryst}. This docking result predicted the binding conformation of INH-NAD inhibitor **3** with a RMSD of 0.6 Å from the conformation obtained with X-ray crystallographic

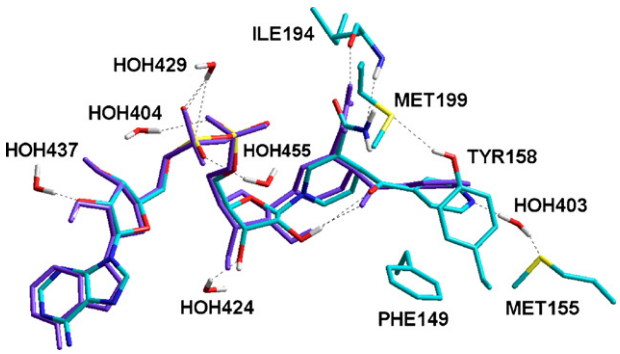

Fig. 3. Superimposition of the conformation **3**^{cryst} crystallized in the InhA pocket (CPK atom colored representation) and the more stable conformation **3**^{calc} (purple) calculated with Autodock. Non-polar hydrogens are not displayed for clarity.

Table 2
Crystallographic and calculated data on possible stacking between the isonicotinic pyridine ring of adducts and the aromatic ring of Phe149.

	Distance (Å)[a]			Dihedral angle (°)[b]		
3^{cryst}	4.2			8.5		
	Autodock	AM1	ONIOM	Autodock	AM1	ONIOM
3^{calc}	4.5	4.1	3.7	38	3	12
4	–	5.5	4.4	–	51	45.5
6	–	4.8	3.8	–	20	16
7	–	3.9	4.2	–	12	26

[a] Calculated from ring centers of pyridine ring of adduct and phenyl of Phe149.
[b] Calculated between the planes of pyridine ring of adduct and phenyl of Phe149.

studies. The NADH and NAD^+ cofactors, docked in the same conditions as the adduct **3**, exhibited energies of −18.5 and −17.7 kcal/mol, respectively (Table 1). According to these results, affinity for the InhA target was in the expected increasing order: NAD^+ < NADH < INH-NAD. These results are in qualitative accordance (if we consider the relative ranking) with experimental data from literature in which the binding affinity constants of ligands to InhA are in the following range: NAD^+ K_i = 4 mM, NADH K_D = 2 μM, and INH-NAD K_d or K_i = 0.4–100 nM (Table 1).

The whole of these data affords a preliminary validation of the Autodock model to study interactions of INH-NAD adducts and analogues with InhA. Docking studies were then performed including all the compounds **1**–**9** described in Table 1. However, in empirical molecular mechanics methods, electronic interactions are only partly described. Thus, in a complementary study, quantum mechanics approaches were also applied. The hybrid quantum mechanics/molecular mechanics (QM/MM) methods allow to treat a part of a large system at a very accurate level and to estimate interaction energy between a ligand and a whole protein. Nevertheless this methodology cannot easily applied to studies involving several tens of compounds for reasons of computational cost and tedious atomic parametrization. Semi-empirical calculations cannot moreover be considered on the whole systems. As our aim was to conceive a model readily usable, we only considered the amino acid residues, which encompass ligands at the level of the catalytic cavity of InhA and in which the relaxed ligand was inserted. A gradient energy calculation (single point calculation) was then performed using the AM1 [38] Hamiltonian for all compounds **1**–**9**. The good potentiality of this semi-empirical method to estimate the interaction enthalpies of ligands in a protein environment was recently depicted [57]. On the other hand, ONIOM (QM/MM) hybrid calculations [43,44] were performed for comparison on the whole flexible system for some compounds.

Results obtained for each compound with Autodock, AM1 and ONIOM are given in Table 1 and are commented in the next paragraphs. For clarity, interaction energies are given relative to the lowest energy value, which was found for **3**^{calc} whatever was the method. Details on calculated binding energies of compounds **3**, **4**, **6** and **7** with MM/GBSA are presented in the molecular dynamics paragraph. Neither entropic nor desolvation terms were considered with AM1 and ONIOM methods. Indeed the time and the memory needed to access to the thermodynamic parameters were dissuasive. Considering the calculated data, one can notice large variation in interaction energies depending on the method and also high-interaction energies found by the two methods. The energies range between −160 and −110 kcal/mol with AM1 and between −531 and −395 kcal/mol with ONIOM (in the later case, there was a full optimization). In order to compare these energy values, we performed single point calculations at the AM1 and the ONIOM levels with some adducts in similar conditions. In these cases, InhA and adduct structures were kept rigid. We observed that there was a coefficient of about two between the results from the two methods (i.e. −129 kcal/mol vs. −255 kcal/mol for **3**^{cryst} at the AM1 and ONIOM levels, respectively). An analogous fact was yet depicted in a study performed on an antifreeze protein interacting with water molecules [58] and the variations are explained by differences in the algorithms used. The high-interaction energies that we obtained by both QM methods could be explained in part by strong interactions generated by the two negative charges of the pyrophosphate moiety [57].

3.1. Comments on conformations 3^{cryst} and 3^{calc} of chain 4S adduct 3, and on conformation of chain 4R adduct 4

In addition to Autodock calculations, the interaction energies were estimated using the AM1 Hamiltonian on a rigid model of the InhA protein after a molecular mechanics relaxation of the adducts in the catalytic cavity. An ONIOM full optimization was moreover performed. These two last methods gave the lower binding energy for the 4*S* adduct **3** (−159.5 kcal/mol and −531 kcal/mol, respectively). Interaction energies of adducts **4**–**9** (Table 1) are expressed as relative values against adduct **3**^{calc} taken as reference. As example, relative interaction energies ($\Delta E_{relative}$) of the chain 4*R* adduct **4** were found 11.1 and 23 kcal/mol for AM1 and ONIOM methods, respectively. This is in qualitative accordance with the results obtained with Autodock ($\Delta E_{relative}$ of **4** = 2 kcal/mol, in favour of **3**^{calc}). Since the binding energy of 4*R* adduct **4** is higher than that of the 4*S* isomer **3** (Table 1), it would be predicted a better interaction of the 4*S* adduct with the InhA target. By the three methods of calculations (docking, AM1 and ONIOM), it was found that the 4*R* adduct **4** is positioned in the active site in almost the same way as 4*S* adduct **3** but with the carbonyl of the isonicotinoyl group oriented in an opposite direction. It is interesting to note that the conformation of **3**^{calc} (Fig. 4) and its main interactions with InhA using the two methods AM1 and ONIOM are quite similar to those described by Rozwarski et al. for the crystal conformation **3**^{cryst} [10].

One can particularly mention the π–π stacking interaction of the pyridine ring of the isonicotinoyl fragment with the side chain of Phe149: distances and dihedral angles of the two aromatic structures are very similar for AM1 and ONIOM calculated conformations and in the crystal structure (Table 2) while in Autodock conformation the two aromatic rings are not parallel (dihedral angle 38°) and are spaced out of about 4.5 Å. Among some minor differences between the crystalline and the calculated conformations we can note that H-bonding through water 403 is found between the nitrogen atom of pyridine ring and either the sulphur atom of Met155 (adduct **3**^{cryst} and 4*R* adduct **4**) or the carbonyl oxygen atom of Asp150 (4*S* adduct **3**^{calc}) (Fig. 5). Also H-bonding interactions of the amido NH_2 group of nicotinamide with Ile194 is maintained although slight differences between **3**^{calc}, **4** and **3**^{cryst} can be noticed.

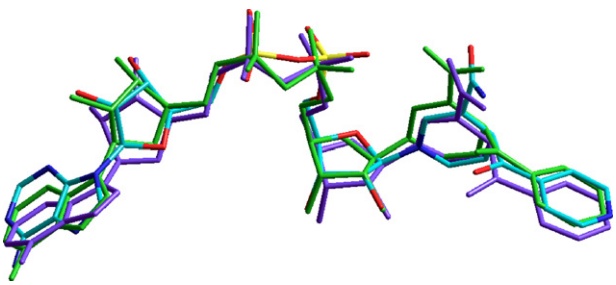

Fig. 4. Superimposition of the conformations **3**^{cryst} (CPK atom colored representation) and **3**^{calc} issued from ONIOM (purple) or AMMP (green).

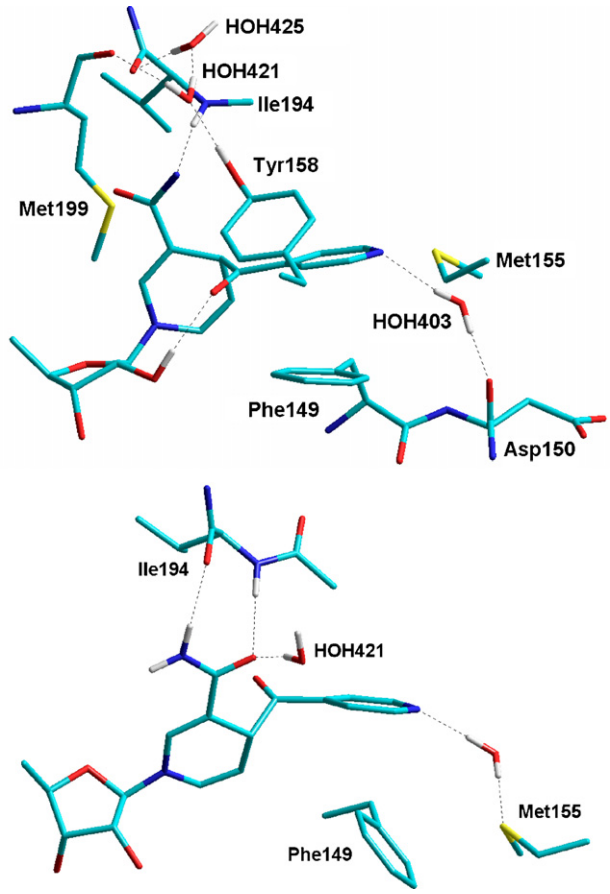

Fig. 5. The main interactions between the isonicotinoyl nicotinamide part of $\mathbf{3}^{calc}$ (top) and **4** (bottom) adducts and the InhA environment found in the flexible ONIOM model.

Although H-bonding with water403 cannot exist in the case of the analogue BH-NAD **5** (replacement of the isonicotinoyl moiety by a benzoyl group), the Autodock results did not show significant differences between INH-NAD adduct $\mathbf{3}^{calc}$ and analogue **5** with respect to docking affinities into the binding site (Table 1, −24.0 and −23.3 kcal/mol, respectively). AM1 and ONIOM calculations led us to the same conclusion.

3.2. Comments on ring 4S,7R adduct 6 and 4R,7S adduct 7

The ring adducts **6** and **7** exhibited a very similar energy of interaction in the binding site of InhA in both AM1 and ONIOM calculations (Table 1, $\Delta E_{relative}$ = 5.1 and 6.2 kcal/mol, 47 and 55 kcal/mol, respectively). These energies of interaction are clearly higher than those of the chain adducts $\mathbf{3}^{calc}$ and **5** (both with configuration 4*S*) whatever the method used. This may be due to the constrained structure of the ring structure as compared to the flexible structure of the chain adducts. In the presence of the ring hemiamidal moiety, changing the configurations from 4*S*,7*R* (adduct **6**) to 4*R*,7*S* (adduct **7**) leads to a rotation of the rigid bicyclic group (dihydronicotinamide-hemiamidal ring) of about 60° around the C(ribose)-*N*(dihydronicotinamide) bond. Even so, their calculated binding energies were very similar, unlike binding energies of chain 4*S* and 4*R* adducts **3** and **4** that were clearly different (Table 1). For both compounds **6** and **7**, the π–π stacking interaction of the isonicotinic ring with the phenyl of Phe149 (favourable distance and dihedral angle, Table 2), the H-bonding to Met155 through water403 and also the H-bonding with Ile194 were found retained. The main difference between these two adducts, is that the 7-OH H-bond interaction with Tyr158 is only present for the 4*S*,7*R* adduct **6** and is not observed for the 4*R*,7*S* diastereoisomer **7**. It is interesting to note that when 7-OH is removed and replaced by 7-H (see footnotes [e] and [f] in Table 1), the binding energy is mainly increased (+2.9 kcal/mol) in the case of **6** where 7-OH H-bond with Tyr158 can exist (Fig. 6 top and middle) while the energy is only weakly affected (by −1 kcal/mol) in the case of **7** where H-bond with Tyr158 is not possible (Fig. 6 bottom).

It is worth to note that the very small difference of energy of interaction between the two ring diastereoisomers **6** and **7** when calculated either by AM1 or by ONIOM is in contrast with our previous experimental data [17] in which the two isomers have shown significant different inhibitory activities towards InhA (Table 1). This point will be discussed later in this article.

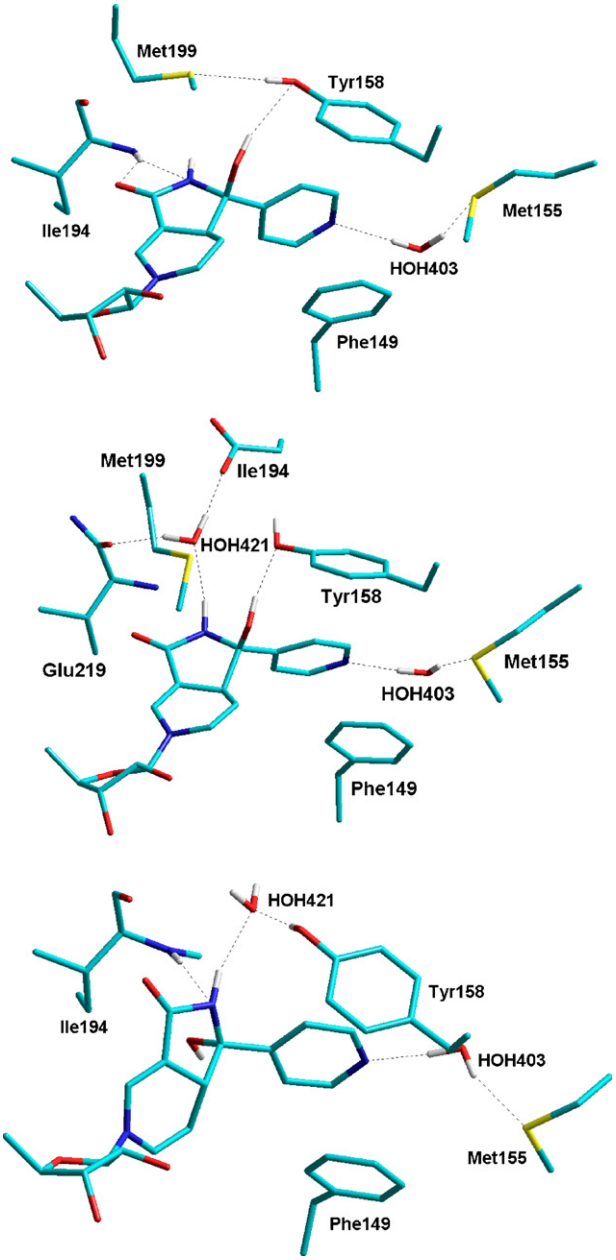

Fig. 6. The main interactions between the isonicotinoyl nicotinamide part of the 4*S*,7*R* **6** (top, AMMP model and middle, ONIOM model) and 4*R*,7*S* **7** (bottom, ONIOM model) adducts and the InhA environment.

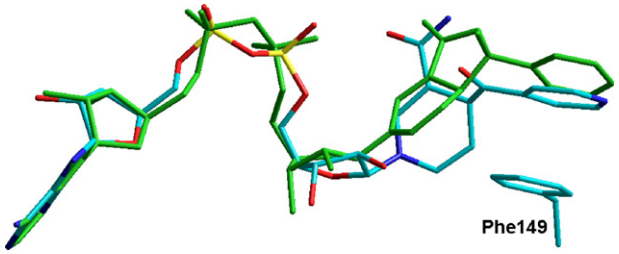

Fig. 7. Superimposition of the AMMP calculated conformations of the 4*S* adduct **3** (CPK atom colored representation) and of the 4*S*,7*R* adduct **6** (green).

The superimposition of the AMMP calculated conformations of the 4*S* adduct **3** and of the 4*S*,7*R* adduct **6** is shown in Fig. 7 for information.

3.3. Comments on oxidized adducts 8 and 9

The AM1 energies of interaction of the oxidized adducts **8** and **9** (pyridinium type) increases significantly ($\Delta E_{relative}$ = 35 and 50 kcal/mol) when compared with all the reduced dihydropyridine adducts **3**–**7**. These calculated energies are coherent with the value determined with the pyridinium cofactor NAD^+ itself ($\Delta E_{relative}$ = 29 kcal/mol) and correlate well with our previous experiments [16,17] in which no InhA inhibition could be detected for compounds **8**/**9**.

3.4. Molecular dynamics study

Molecular dynamics (MD) simulation studies on the wild-type InhA and isoniazid-resistant Ile21Val and Ile16Thr InhA mutants in complex with the NADH molecule have been successfully employed to identify the NADH affinity differences between wild-type and mutants InhA and better understand the specific molecular mechanisms of INH resistance. Mainly, it was predicted that Ile21Val and Ile16Thr mutations could affect binding of the cofactor pyrophosphate moiety and that the resulting lower affinity could contribute to the drug resistance [59]. In order to confirm the tendency that the 4*S* chain adduct **3** is more energetically favourable to interact with InhA than the 4*S*,7*R* ring adduct **6**, a MD approach was carried out. To estimate the MD trajectory quality and convergence, the fluctuation in potential energy and the RMSD of backbone's atoms from the starting crystal structure (1ZID) were monitored during the MD simulation time.

As shown in Fig. 8 (left), after 3 ns of MD the progression of the RMSD deviation of the protein backbone remained stable suggesting adequate system equilibration during the sampling time. Over the last 4 ns the average value of RMSD was 1.9 ± 0.1 Å. Furthermore it has been checked that the main distance between InhA amino acid groups and 4*S* adduct **3** obtained experimentally in the crystal and theoretically by MD were in good agreement (see supplementary material). A MD simulation time of 9 ns was also achieved for 4*S*,7*R* adduct **6** in respect to the protocol described previously. The starting complex formed by **6** and InhA was obtained from docking calculations with Autodock as described above. For this complex a plateau of the backbone RMSD around 1.8 ± 0.1 Å was reached over the last 5 ns of trajectory (Fig. 8, right).

In order to compare the binding energies obtained by previous theoretical methods with those of structures from simulation by molecular dynamics in explicit water, we used a post-processing method MM/GBSA provided by Amber 7.0 suite [60]. This method consists in calculating free-binding energy by averaging different energy terms over snapshots from MD simulations. The water molecules present in the MD simulation are then replaced by a continuum electrostatic model, in this case based on the so-called "Generalized Born Approach and Solvent Accessibility" and on the addition of a cavity term calculated on the basis of atomic accessible surface areas. The standard MM/GBSA method allows calculation of binding energy as a difference between the energy of the adduct–InhA complex and the energy of individual species. Results for the two adducts **3** and **6** are included in Table 1. Binding energy for 4*S*,7*R* adduct **6** was calculated for the last 5 ns of MD. The calculated binding energy was found more favourable for 4*S* adduct **3** by 4.2 kcal/mol as compared to 4*S*,7*R* adduct **6**. This result is in agreement with binding energies calculated by AM1 and ONIOM methods (Table 1).

On the basis of this background (calculation results showing the chain 4*S* adduct **3** a better ligand than ring 4*S*,7*R* adduct **6**) and taking into account (i) that ring adducts are the major tautomers present in solution [15], (ii) that they were found active InhA inhibitors and (iii) that INH-NAD adducts were described as slow tight-binding inhibitors [19], we hypothesized that the first interaction of the INH-NAD inhibitor with InhA could initially occur through the ring adduct **6** which then tautomerises to give the chain adduct **3** that is energetically more favoured than **6** to interact with InhA. Similarly ring adduct **7** could bind to InhA but either tautomerisation cannot occur (see below) or it leads to the inactive or poorly active chain adduct **4** (not significant difference of interaction energies between **7** and **4**). It is interesting to note that both the flexible AMMP and ONIOM methods showed an hydrogen bond between the tertiary hydroxyl of the 4*S*,7*R* adduct **6** and the phenolic oxygen atom of Tyr158 (Fig. 6 top and middle). In contrast, a similar interaction is not observed for the 4*R*,7*S* adduct **7** with both ONIOM (Fig. 6 bottom) and AMMP methods.

The molecular dynamics study has confirmed that the phenolic oxygen atom of Tyr158 is close to the hydroxylic proton of the hemiamidal structure. In more than 39% of last 5 ns of MD, these

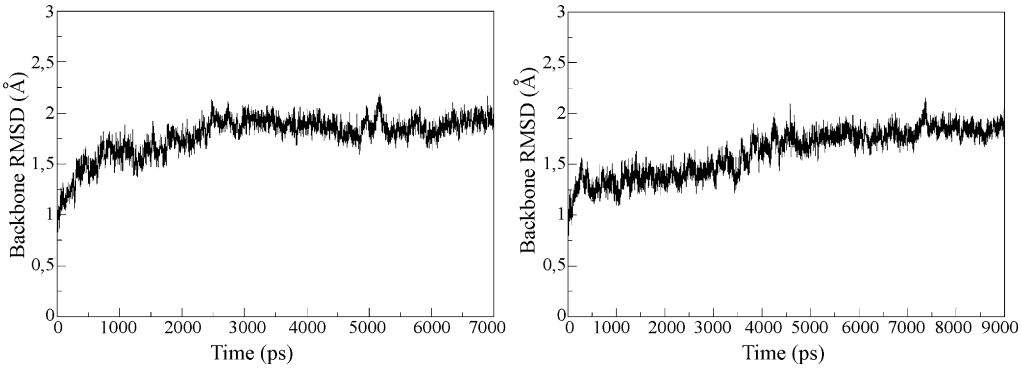

Fig. 8. Backbone RMSD of complex InhA-adduct **3** (left) and InhA-adduct **6** (right) according to the MD simulation time.

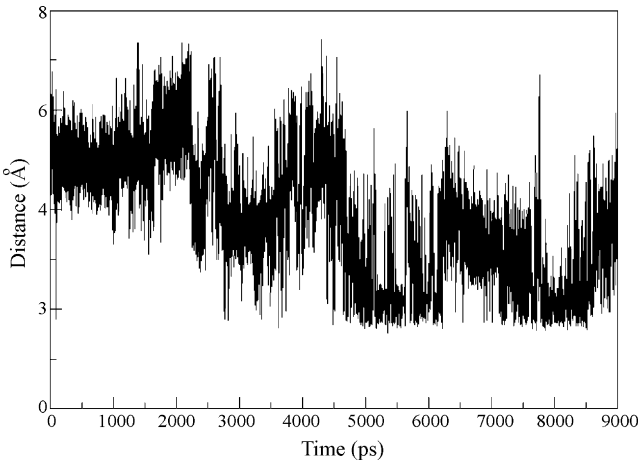

Fig. 9. Time dependence of distance between the phenolic oxygen atom of Tyr158 and the hydroxylic proton of the hemiamidal structure.

groups were spatially very close (Fig. 9) with an average distance of 2.8 Å for this period of time.

These observations allow us to propose a mechanism of opening of the hemiamidal ring catalyzed by Tyr158. One can suppose that the hydroxyl group of Tyr158 interacts both with the sulphur atom of Met199 and with the H-atom of the hemiamidal hydroxyl group of adduct **6** (Scheme 1). In this model, Tyr158 could play a critical role acting as H-donor/H-acceptor as follows: the transitory activated (with assistance of Met199) phenolate of Tyr158 deprotonates the tertiary hydroxyl group of the INH-NAD adduct **6** leading to an alkoxide intermediate which is then converted into the chain (keto-amide) adduct **3** by transfer of a proton from the protonated Met199 to the imidate anion (Scheme 1). Alternatively, activation of Tyr158 could be performed by a water molecule found in the active site of the InhA enzyme instead of by Met199. Indeed, MD simulation showed that there is a water molecule (water 425) close to Tyr158 in more than 35% of the first 4 ns of the experience.

This hypothesis could explain why ring adducts **6** (4*S*,7*R*) and **7** (4*R*,7*S*), having comparable energy of interaction when calculated by AM1 and ONIOM, exhibit experimentally different inhibitory activity. Indeed, the opening of the hemiamidal ring of the 4*S*,7*R* diastereoisomer could be achieved inside the InhA catalytic site by catalysis of Tyr158 to give the 4*S* chain adduct that is more energetically favoured for InhA binding.

On the other hand, the same opening process would not occur with the 4*R*,7*S* adduct since the hemiamidal tertiary hydroxyl in this configuration is pushed on the other side of the hemiamidal bicyclic plane (Fig. 6 bottom), too far from Tyr158 and from other possible catalytic basic residues (H-bond is possible with the carbonyl of Ala191 but the basicity of this group is clearly lower than that of the tyrosine phenolate).

Moreover, this hypothesis can be supported by the known decrease of isoniazid activity observed when Tyr158 is replaced by a Phe residue [61,62]. Indeed, absence of the phenolic hydroxyl group in the Tyr158Phe mutant keeps away from the possibility of the opening process to occur. Since conformation of $\mathbf{3}^{calc}$ inside the InhA active site (Fig. 10) and the AM1 calculated energies of **3** and **6** (+1.6 to +2.3 kcal/mol; Table 3) are only slightly modified by the mutation, decreased activity of INH on the mutant-type InhA could

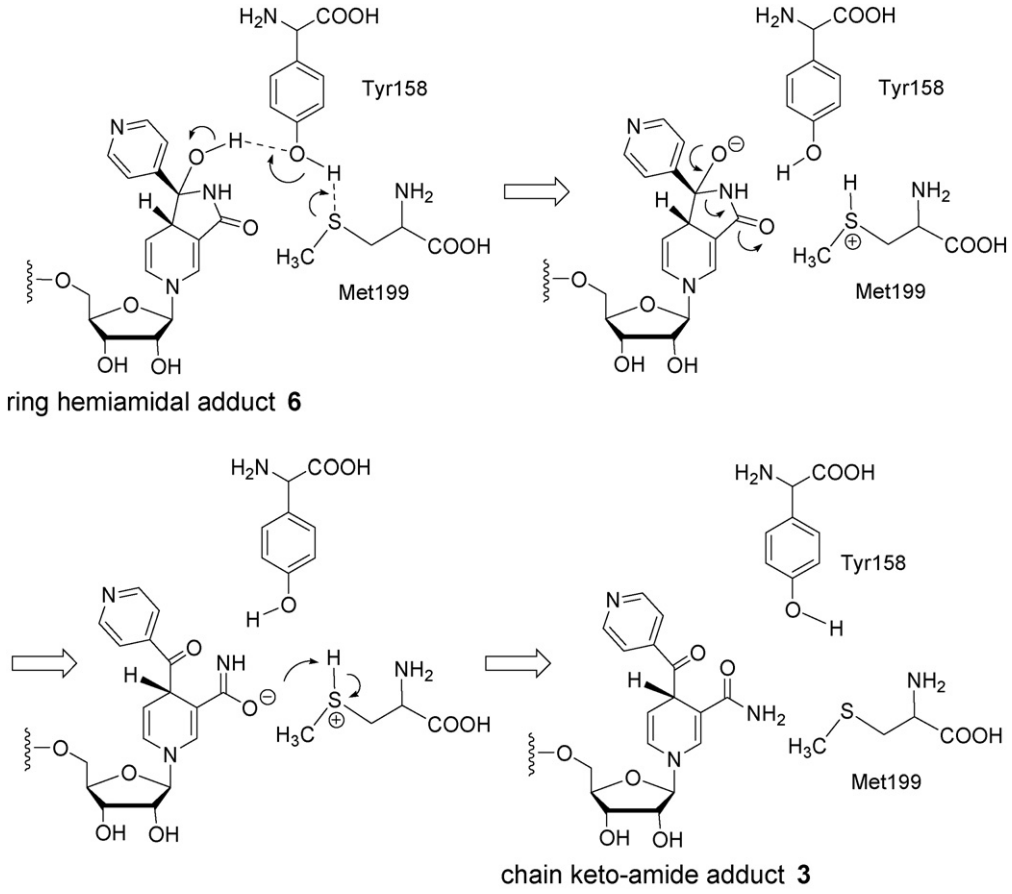

Scheme 1. Proposed mechanism for conversion of the ring tautomer **6** to the chain tautomer **3** involving basic catalysis by Tyr158 and assistance of Met199.

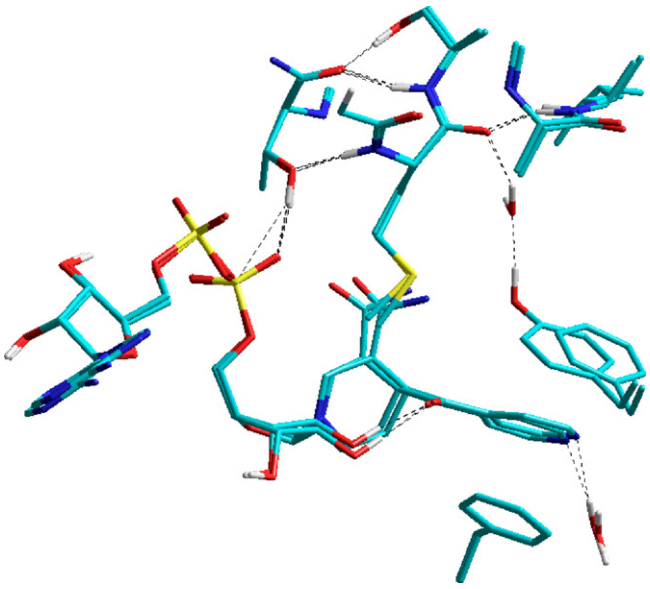

Fig. 10. Comparison of conformations of the 4*S* adduct $\mathbf{3}^{calc}$ in wild-type InhA and in Tyr158Phe mutated InhA.

Table 3
Binding energies of adducts **3** and **6** to wild-type and mutant-type InhA calculated with AM1 method.

	Binding energy (kcal/mol)	
	Wild-type InhA	Tyr158Phe mutant-type InhA
4S chain adduct $\mathbf{3}^{calc}$	−162.5	−160.9
4S,7R ring adduct **6**	−154.4	−152.1

be better explained by the wild-type strain being able to catalyze opening of the hemiamidal ring to give the final active chain adduct **3**, while the mutant-type InhA cannot do that.

4. Conclusion

Up to now, only limited data at the molecular level is available on the interactions of INH-NAD(P) adducts with the proposed isoniazid target proteins. The main reports concern the early crystallographic study of the InhA:INH-NAD adduct complex [10] and, very recently, description of the crystallized InhA:INH-NADP adduct complex [63]. In both cases, a 4*S* chain adduct was evidenced in the active site of the protein. Interestingly, another example concerns the dihydrofolate reductase (DHFR) of *M. tuberculosis*, which was inhibited by the 4*R* chain INH-NADP adduct and the crystal structure of the complex was solved [14]. Based on the X-ray structure of InhA:INH-NAD complex, very few modelling studies were performed, mainly to select relevant descriptors of the biological activity and for structure-based design of new antituberculosis agents (see Section 1 [20–22]).

In this work, a theoretical approach was performed towards a better understanding of the activated species formed from isoniazid and now considered as responsible for the activity of this antituberculosis prodrug in vivo. Main interactions with the target enzyme InhA of ring and chain tautomers of the INH-NAD adducts are described in terms of binding energy, key binding site residues, role of the stereochemistry through studies using computer docking, quantum mechanics molecular mechanics and molecular dynamic methods. Confrontation of experimental data and theoretical results allowed us to compare several methods of calculation and to rationalize the interactions between the different known species of INH-NAD adducts. The best binding energy was observed for the 4*S* chain adduct. It probably represents the effective active form of the INH-NAD adducts, as expected from its early description in a crystallized InhA:INH-NAD complex [10]. The 4*S*,7*R* and 4*R*,7*S* ring tautomers, the two main species that can be observed in solution, show intermediate and similar calculated binding energies contrasting with their different experimental inhibitory potency on InhA. We formulated the hypothesis of an initial binding of the ring tautomers to InhA, followed by opening of only the ring hemiamidal 4*S*,7*R* tautomer catalyzed by Tyr158 phenolate basic group to give the 4*S* chain INH-NAD tight-binding inhibitor. The adducts of a pyridinium type that are biologically inactive showed logically weak calculated binding energies. The models and procedures proposed will be used in prediction of ligand–protein interactions at the molecular level. Beyond its primary importance in elucidating the mechanisms of action of isoniazid and InhA-related resistances to this drug, this work may help to choice a convenient theoretical method to predict the mode and the interaction energy of selective InhA ligands in order to identify the most effective pharmacophore fragments for designing new potential antitubercular drugs.

Acknowledgement

We thank Dr. A. Quémard (IPBS CNRS, France) for very helpful comments just as CALMIP (calcul intensif en Midi-Pyrenees, Toulouse, France) for computing facilities.

Appendix A. Supplementary data

Supplementary data associated with this article can be found, in the online version, at doi:10.1016/j.jmgm.2008.09.006.

References

[1] K. Bartmann, H. Iwainsky, H.H. Kleeberg, P. Mison, H.A. Offe, H. Otten, D. Tettenborn, L. Trnka, Antituberculosis Drugs, Springer-Verlag, Berlin-Germany, 1988.
[2] J.S. Blanchard, Annu. Rev. Biochem. 65 (1996) 215–239.
[3] Y. Zhang, B. Heym, B. Allen, D. Young, S. Cole, Nature 358 (1992) 591–593.
[4] K. Johnsson, P.G. Schultz, J. Am. Chem. Soc. 116 (1994) 7425–7426.
[5] J.A. Marcinkeviciene, R.S. Magliozzo, J.S. Blanchard, J. Biol. Chem. 270 (1995) 22290–22295.
[6] K. Johnsson, W.A. Froland, P.G. Schultz, J. Biol. Chem. 272 (1997) 2834–2840.
[7] J.-Y. Wang, R.M. Burger, K. Drlica, Antimicrob. Agents Chemother. 42 (1998) 709–711.
[8] A. Quémard, A. Dessen, M. Sugantino, W.R. Jacobs, J.C. Sacchettini, J.S. Blanchard, J. Am. Chem. Soc. 118 (1996) 1561–1562.
[9] H. Marrakchi, G. Laneelle, A. Quémard, Microbiology 146 (2000) 289–296.
[10] D.A. Rozwarski, G.A. Grant, D.H.R. Barton, W.R. Jacobs Jr., J.C. Sacchettini, Science 279 (1998) 98–102.
[11] B. Lei, C.-J. Wie, S.-C. Tu, J. Biol. Chem. 275 (2000) 2520–2526.
[12] M. Nguyen, C. Claparols, J. Bernadou, B.C.R. Meunier, Chimie 5 (2002) 325–330.
[13] M. Wilming, K. Johnsson, Angew. Chem. Int. Ed. 38 (1999) 2588–2590.
[14] A. Argyrou, M.W. Vetting, B. Aladegbami, J.S. Blanchard, Nat. Struct. Mol. Biol. 13 (2006) 408–413.
[15] M. Nguyen, C. Claparols, J. Bernadou, B. Meunier, ChemBioChem 2 (2001) 877–883.
[16] S. Broussy, V. Bernardes-Génisson, Y. Coppel, A. Quémard, J. Bernadou, B. Meunier, Org. Biomol. Chem. 3 (2005) 670–673.
[17] M. Nguyen, A. Quémard, S. Broussy, J. Bernadou, B. Meunier, Antimicrob. Agents Chemother. 46 (2002) 2137–3144.
[18] T. Delaine, V. Bernardes-Génisson, J.-L. Stigliani, H. Gornitzka, B. Meunier, J. Bernadou, Eur. J. Org. Chem. (2007) 1624–1630.
[19] R. Rawat, A. Whitty, P. Tonge, Proc. Natl. Acad. Sci. U.S.A. 100 (2003) 13881–13886.
[20] K.F.M. Pasqualoto, E.I. Ferreira, O.A. Santos-Filho, A.J. Hopfinger, J. Med. Chem. 47 (2004) 3755–3764.
[21] K.F.M. Pasqualoto, M.M.C. Ferreira, O.A. Santos-Filho, A.J. Hopfinger, Int. J. Quantum Chem. 106 (2006) 2689–2699.
[22] L. Bonnac, G.Y. Gao, L. Chen, K. Felczak, E.M. Bennett, H. Xu, T.S. Kim, N. Liu, H.W. Oh, P.J. Tonge, K.W. Pankiewicza, Bioorg. Med. Chem. Lett. 17 (2007) 4588–4591.

[23] S. Broussy, V. Bernardes-Génisson, H. Gornitzka, J. Bernadou, B. Meunier, Org. Biomol. Chem. 3 (2005) 666–669.
[24] S. Broussy, V. Bernardes-Génisson, A. Quémard, B. Meunier, J. Bernadou, J. Org. Chem. 70 (2005) 10502–10510.
[25] T. Delaine, V. Bernardes-Génisson, B. Meunier, J. Bernadou, J. Org. Chem. 72 (2007) 675–678.
[26] S.C. Lovell, I.W. Davis, W.B. Arendall III, P.I.W. de Bakker, J.M. Word, M.G. Prisant, J.S. Richardson, D.C. Richardson, Proteins: Struct. Funct. Genet. 50 (2003) 437–450.
[27] A. Pedretti, L. Villa, G. Vistoli, J. Mol. Graph. 21 (2002) 47–49.
[28] R.W. Harrison, J. Comp. Chem. 14 (1993) 1112–1122.
[29] G.M. Morris, D.S. Goodsell, R.S. Halliday, R. Huey, W.E. Hart, R.K. Belew, A.J. Olson, J. Comp. Chem. 19 (1998) 1639–1662.
[30] A. Dessen, A. Quémard, J.S. Blanchard, W.R. Jacobs Jr., J.C. Sacchettini, Science 267 (1995) 1638–1641.
[31] D.A. Rozwarski, C. Vilcheze, M. Sugantino, R. Bittman, J.C. Sacchettini, J. Biol. Chem. 274 (1999) 15582–15589.
[32] W.H. Miller, M.A. Seefeld, K.A. Newlander, I.N. Uzinskas, W.J. Burgess, D.A. Heerding, C.C. Yuan, M.S. Head, D.J. Payne, S.F. Rittenhouse, T.D. Moore, S.C. Pearson, V. Berry, W.E. DeWolf Jr., P.M. Keller, B.J. Polizzi, X. Qiu, C.A. Janson, W.F. Huffman, J. Med. Chem. 45 (2002) 3246–3256.
[33] R. Perozzo, M. Kuo, A.S. Sidhu, J.T. Valiyaveettil, R. Bittman, W.R. Jacobs Jr., D.A. Fidock, J.C. Sacchettini, J. Biol. Chem. 277 (2002) 13106–13114.
[34] M.F. Sanner, B.S. Duncan, C.J. Carillo, A.J. Olson, Pac. Sympos. Biocomput. (1999) 401–412.
[35] AutoDockTools. Molecular Graphics Laboratory, Scripps Research Institute, La Jolla, California. Available from http://www.scripps.edu/~sanner/python/.
[36] B.H. Besler, K.M. Merz Jr., P.A. Kollman, J. Comp. Chem. 11 (1990) 431.
[37] M.J. Frisch, G.W. Trucks, H.B. Schlegel, G.E. Scuseria, M.A. Robb, J.R. Cheeseman, J.A. Montgomery, T. Vreven Jr., K.N. Kudin, J.C. Burant, J.M. Millam, S.S. Iyengar, J. Tomasi, V. Barone, B. Mennucci, M. Cossi, G. Scalmani, N. Rega, G.A. Petersson, H. Nakatsuji, M. Hada, M. Ehara, K. Toyota, R. Fukuda, J. Hasegawa, M. Ishida, T. Nakajima, Y. Honda, O. Kitao, H. Nakai, M. Klene, X. Li, J.E. Knox, H.P. Hratchian, J.B. Cross, V. Bakken, C.J. Adamo, J. Jaramillo, R. Gomperts, R.E. Stratmann, O. Yazyev, A.J. Austin, R. Cammi, C. Pomelli, J.W. Ochterski, P.Y. Ayala, K. Morokuma, G.A. Voth, P. Salvador, J.J. Dannenberg, V.G. Zakrzewski, S. Dapprich, A.D. Daniels, M.C. Strain, O. Farkas, D.K. Malick, A.D. Rabuck, K. Raghavachari, J.B. Foresman, J.V. Ortiz, Q. Cui, A.G. Baboul, S. Clifford, J. Cioslowski, B.B. Stefanov, G. Liu, A. Liashenko, P. Piskorz, I. Komaromi, R.L. Martin, D.J. Fox, T. Keith, M.A. Al-Laham, C.Y. Peng, A. Nanayakkara, M. Challacombe, P.M.W. Gill, B. Johnson, W. Chen, M.W. Wong, C. Gonzalez, J.A. Pople, Gaussian 03, Revision B.05, Gaussian, Inc, Wallingford CT, 2004.
[38] M.J.S. Dewar, E.G. Zoebisch, E.F. Healy, J.J.P. Stewart, J. Am. Chem. Soc. 107 (1985) 3902–3909.
[39] J.J.P. Stewart, J. Comp. Chem. 10 (1989) 209–220.
[40] A.A. Granovsky, http://www.classic.chem.msu.su/gran/gamess/index.html.
[41] M.W. Schmidt, K.K. Baldridge, J.A. Boatz, S.T. Elbert, M.S. Gordon, J.J. Jensen, S. Koseki, N. Matsunaga, K.A. Nguyen, S. Su, T.L. Windus, M. Dupuis, J.A. Montgomery, J. Comput. Chem. 14 (1993) 1347–1363.
[42] P. Pulay, Chem. Phys. Lett. 73 (1980) 393–398.
[43] F. Maseras, K. Morokuma, J. Comp. Chem. 16 (1995) 1170–1179.
[44] S. Dapprich, I. Komaromi, S. Byun, K. Morokuma, M.J. Frisch, J. Mol. Struct. (THEOCHEM) 461 (1999) 1–23.
[45] A.D. Becke, J. Chem. Phys. 98 (1993) 5648–5652.
[46] W.D. Cornell, P. Cieplak, C.I. Bayly, I.R. Gould, K.M. Merz Jr., D.M. Ferguson, D.C. Spellmeyer, T. Fox, J.W. Caldwell, P.A. Kollman, J. Am. Chem. Soc. 117 (1995) 5179–5197.
[47] R. Dennington II, T. Keith, J. Millam, K. Eppinnett, W.L. Hovell, R. Gilliland, GaussView, Version 3.09, Semichem, Inc., Shawnee Mission, KS, 2003.
[48] J. Wang, R.M. Wolf, J.W. Caldwell, P.A. Kollman, D.A. Case, J. Comput. Chem. 25 (2004) 1157–1174.
[49] C.I. Bayly, P. Cieplak, W.D. Cornell, P.A. Kollman, J. Phys. Chem. 97 (1993) 10269–10280.
[50] H.J.C. Berendsen, J.P.M. Postma, W.F. van Gunsteren, A. DiNola, J.R. Haak, J. Comput. Phys. 81 (1984) 3684–3690.
[51] J.P. Rychaert, G. Ciccotti, H.J.C. Berendsen, J. Comput. Phys. 23 (1977) 327–341.
[52] T.A. Darden, D. York, L.G. Pedersen, J. Chem. Phys. 98 (1993) 10089–10092.
[53] U. Essmann, L. Perera, M.L. Berkowitz, T. Darden, H. Lee, L.G. Pedersen, J. Chem. Phys. 103 (1995) 8577–8593.
[54] M.F. Sanner, A.J. Olson, J.C. Spehner, Biopolymers 38 (1996) 305–320.
[55] F.W. Humphery, A. Dalke, K. Shulten, J. Mol. Graph. 14 (1996) 33–38.
[56] A. Quémard, J.C. Sacchettini, A. Dessen, C. Vilcheze, R. Bittman, W.R. Jacobs, J.S. Blanchard, Biochemistry 34 (1995) 8235–8241.
[57] R. Villar, M.J. Gil, J.I. Garcia, V. Martinez-Merino, J. Comput. Chem. 26 (2005) 1347–1358.
[58] Z. Yang, Y. Zhou, K. Liu, Y. Cheng, R. Liu, G. Chen, Z. Jia, Biophys. J. 85 (2003) 2599–2605.
[59] K.E. Schroeder, L.A. Basso, D.S. Santos, O.N. de Souza, Biophys. J. 89 (2005) 876–884.
[60] D.A. Case, D.A. Pearlman, J.W. Caldwell, T.E. Cheatham III, J. Wang, W.S. Ross, C.L. Simmerling, T.A. Darden, K.M. Merz Jr., R.V. Stanton, A.L. Cheng, J.J. Vincent, M. Crowley, V. Tsui, H. Gohlke, R.J. Radmer, Y. Duan, J. Pitera, I. Massova, G.L. Seibel, U.C. Singh, P.K. Weiner, P.A. Kollman, Amber 7, University of California, San Francisco, 2002.
[61] S.L. Parikh, D.P. Moynihan, G. Xiao, P. Tonge, J. Biochem. 38 (1999) 13623–13634.
[62] S.L. Parikh, G. Xiao, P. Tonge, J. Biochem. 39 (2000) 7645–7650.
[63] A. Argyrou, M.W. Vetting, J.S. Blanchard, J. Am. Chem. Soc. 31 (2007) 9582–9583.